# New Aspects of the Electroadsorption of Ethyl Xanthate on Copper Electrodes

**Paula Grez, Carlos Celedón, Aurora Molinari, Alfonso Oliva, Marco Orellana, Ricardo Schrebler, Rodrigo del Río, and Ricardo Córdova***

*Instituto de Química, Pontificia Universidad Católica de Valparaíso, Avda. Brasil 2950, Casilla 4059, Valparaíso, Chile*

*Received: August 10, 2005; In Final Form: September 30, 2005*

The interaction of the ethyl xanthate (EX) anion with a copper electrode in a borate buffer solution, pH 9.2, has been investigated by cyclic voltammetry (CV), electrochemical quartz crystal microbalance (EQCM), electrochemical impedance spectroscopy (EIS), and measurements of contact angle (CA) under controlled potential. The results obtained allow establishing that, in the potential range from −0.80 and −0.60 V, two parallel reactions were characterized. These reactions were the ethyl xanthate electroadsorption and the hydrogen evolution reaction (HER). This last reaction has not been described by previous authors. Besides, the EIS measurements show that the mechanism of the HER on copper electrodes is not affected by the presence of a ethyl xanthate species. The EQCM study shows that in the electrodesorption process the departure of each ethyl xanthate species from the copper electrode is accompanied with the simultaneous entry of four to five water molecules. This fact is in accordance with the number of copper atoms involved in the adsorption of one ethyl xanthate species.

## Introduction

The interaction of mineral surfaces with surfactant agents (referred to also as collectors) is one of the keys to understanding the flotation process of minerals. Dialkyldithiophosphate (DTP) and alkyldithiocarbonates (usually named as alkyl xanthates) are the most common collector agents employed in the flotation process for sulfide minerals.[1] Both types of collector agents are generally designed as thiol collectors.

However, the study of the interaction of these collector agents with metallic surfaces has been recognized as a model system for obtaining knowledge about the complex electrochemical processes that take place during the flotation of sulfide mineral species with the thiol collectors.

From this point of view, an electrochemical study of the interaction of DTP with a copper, platinum, and chalcocite surface has been performed.[2] The interaction of the alkyl xanthate collectors with platinum and gold,[3] copper,[3−8] lead,[9] silver,[10,11] and mineral surfaces such as chalcocite,[4,12] pyrite and chalcopyrite,[12−14] galena,[3,12,15,16] and a mixture of chalcocite and bornite[17] has also been investigated. In these studies, both electrochemical techniques (cyclic voltammetry,[2−6,9,10,12,13,17] open circuit potential,[4,10] potential step,[6,10] nanoelectrogravimetric,[6] and contact angle[10,13,14] measurements) and surface characterization techniques (Fourier transform infrared (FTIR) spectroscopy,[5,8,10,12] X-ray photoelectron spectroscopy (XPS),[7,11,15,16] surface-enhanced raman spectroscopy (SERS),[11] and UV−visible spectroscopy[8,10,14]) were employed to obtain insight into the nature of the electrochemical processes and to identify the products formed on the electrode surface under the different experimental conditions assayed. In general, the mechanisms by means of which the collectors act on the metal or mineral electrode surface can be expressed by the following global reactions:

$$MS + X^-(aq) \rightarrow MSX_{ads} + e^- \quad (1)$$

$$MS + 2X^-(aq) \rightarrow MSX_{2(ads)} + 2e^- \quad (2)$$

$$MS + 2X^-(aq) \rightarrow MX_{2(ads)} + S_{ads} + 2e^- \quad (3)$$

In these reactions, MS represents a sulfide mineral of the metal M, $X_{ads}$ represents an adsorbed radical species, $X_2$ represents a dimeric species derived from the respective thiol, $MX_2$ represents a metal−collector compound, and S corresponds to elemental sulfur. These species are formed on the surface of mineral particles and contribute to give the necessary hydrophobicity to them that allows its flotation by bubbles under the conditions of the industrial flotation processes.

For the interaction between ethyl xanthate and a copper electrode surface, which has been studied by several authors,[3−8] the following aspects have been described:

In electrochemical experiments, a charge transfer chemisorption process of ethyl xanthate species takes place before the electroformation of the multilayer of copper−ethyl xanthate[3,4,6] and so does in DTP.[2]

Spectroelectrochemical measurements of the electrode surface show that the formation of the copper−ethyl xanthate compound (CuEX) takes place with the ethyl xanthate chain perpendicular to the copper electrode surface.[5]

On the other hand, in borate buffer solutions containing 2 mM ethyl xanthate anion, dixanthogen species are formed when the copper electrode potential is close to 0.0 V (SCE). Spectroelectrochemical measurements show that the dixanthogen species are randomly oriented on the electrode surface.[5]

According to the current work in the potential range where the ethyl xanthate anion ($EX^-$) electrosorption on copper surfaces takes place, a stationary negative current value is always attained. This fact has not been mentioned by previous authors.[4,5] To explain the origin of this stationary negative current observed during the electrosorption of $EX^-$, we postulate that a hydrogen

* Corresponding author. E-mail: rcordova@ucv.cl. Phone: +56 32 273179. Fax: +56 32 273422.

10.1021/jp054477e CCC: $30.25 
Published on Web 11/10/2005

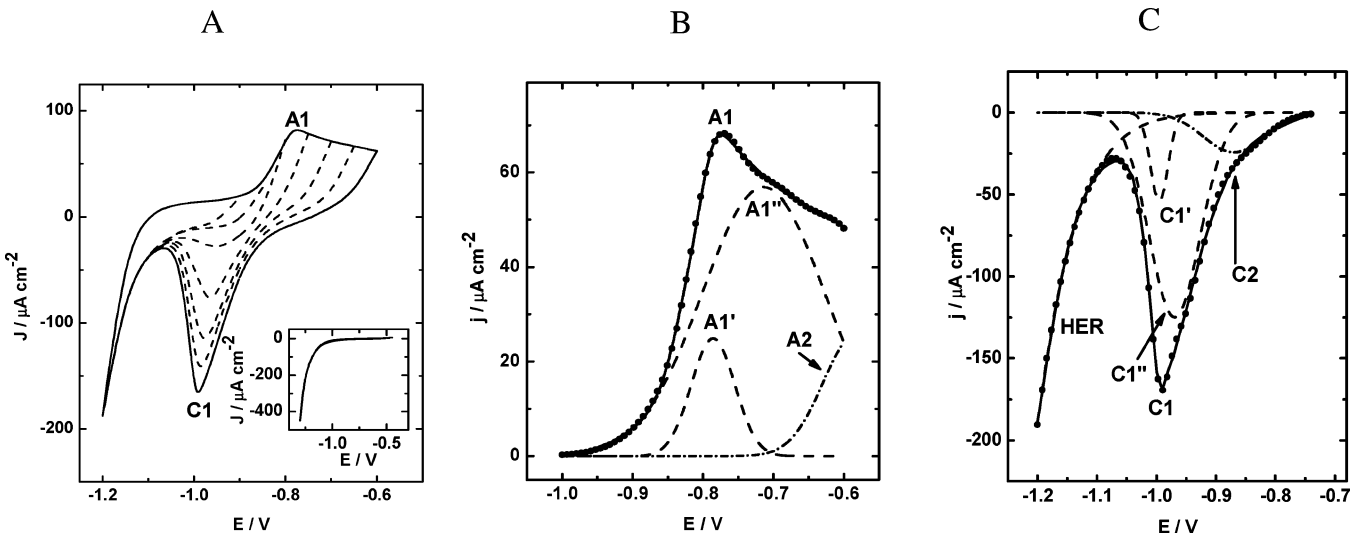


**Figure 1.** (A) Cyclic voltammograms of a bulk copper electrode in 50 mM borate buffer, pH 9.2, in the presence of 1 mM $EX^-$. Scan rate 0.02 V $seg^{-1}$. Inset: blank registered under the same conditions in the absence of $EX^-$. (B) PGPS of part A and the deconvoluted current contributions. (C) NGPS of part A and the deconvoluted current contributions.

evolution reaction (HER) takes place simultaneously with the electrosorption of $EX^-$ and occurs in a greater extension than the last one. Therefore, the aim of the present work is to demonstrate this assumption employing techniques such as cyclic voltammetry (CV), potentiostatic step (PS), electrochemical impedance spectroscopy (EIS), electrochemical quartz crystal microbalance (EQCM), and contact angle measurements (CAMs).

## Experimental Section

A conventional three-electrode electrochemical cell was used. Before each measurement, the electrolyte solution was deaerated with argon for 45 min and then an inert atmosphere was maintained above the solution. According to the techniques employed, different working electrodes were used. In the CV, EIS, and CAM techniques, a bulk copper electrode (0.30 $cm^2$) was employed, and in the EQCM experiments, a thin film of copper electrodeposited on a quartz resonator (Si/Au) with a geometric area of 0.20 $cm^2$ was used. When bulk copper electrodes were employed, they were mechanically polished with 0.05 $\mu$m alumina or chemically polished with a $HNO_3/H_2O$ (1:1) mixture for 30 s. Then, they were rinsed with deionized water before each measurement. A platinum wire and a saturated calomel electrode (SCE, 0.242 V vs NHE) were employed, the former as an auxiliary electrode and the latter as a reference electrode. A buffer solution (50 mM $Na_2B_4O_7$, pH 9.2), containing potassium ethyl xanthate (0 mM $\leq$ [KEX] $\leq$ 1 mM), was employed as the electrolytic medium in all of the experiments. To reduce all of the oxygen-containing copper species formed during the previous treatment of the electrode, a potentiostatic pulse at $-1.3$ V was applied to the electrodes for 5 min, before each measurement. For the ethyl xanthate adsorption measurements, from this conditioning potential, an adsorption potential step ($E_{ads}$) in the range from $-0.900$ to $-0.575$ V was applied for 4 min, allowing the electroadsorption of the EX radical analyte. Then, a negative-going potential scan (NGPS) at a scan rate of 0.02 V $s^{-1}$ was performed from $E_{ads}$ to a cathodic limit potential ($E_{\lambda,C}$) with a value of $-1.3$ V, registering the corresponding *I*/*E* profile. In voltammetric experiments, a cyclic voltammetry program was applied starting from a potential value of $-1.3$ V to an anodic limit potential value ($E_{\lambda,a}$) of $-0.60$ or $-0.45$ V. The same potential range was employed both in the positive-going potential scan (PGPS) and in the negative-going potential scan (NGPS).

In the EQCM experiments, the quartz resonator was an AT-cut quartz crystal resonating at a fundamental frequency of 10 MHz and a sensitivity of 5.8 $ng \cdot cm^{-2} \cdot Hz^{-1}$. Before electrodepositing the copper film on the Si/Au electrode system, it was cleaned with a freshly prepared mixture of $H_2SO_4/HNO_3$ (1:1) for 2 min, followed by a rinse with Milli-Q water. Copper deposition took place when a potential step of $-0.100$ V for 40 s was applied in a 50 mM $CuSO_4$ and 10 mM $Na_2SO_4$, pH 2.0, electrolytic solution. Then, the electrode was mounted in the electrolytic cell, exposing the copper surface to the electrolyte. The changes of mass, potential, and current were measured in an ELCHEMA, model EQCM-501, electrochemical quartz crystal microbalance (EQCM) connected to a Pine Instrument Company, model RDE 4, bipotentiostat and interfaced to a personal computer. The data acquisition and data analysis were performed using the Voltscan 3.0 and Master Window 3.2 software supplied by ELCHEMA.

For EIS measurements, the bulk copper electrode employed was polarized in the potential range from $-0.95$ to $-0.70$ V until a constant current value was attained. Then, a 5 mV root-mean-square (rms) ac signal, with a frequency range from 10 kHz to 10 mHz, was applied using a Zahner, model IM6e, potentiostat/galvanostat. The data acquisition and data analysis were performed using the THALES package from Zahner Elektric GmbH & Co.

Contact angle measurements (CAMs), in the corresponding electrolyte, were done by stepping the potential of a clean copper surface electrode in the potential range from $-1.0$ to $-0.60$ V for 20 min. Afterward, a bubble of argon was placed by means of a syringe on the electrode surface. The argon bubble angles established were measured on both sides of the bubble with an RNL RAME HART, model 100-00-230, angle goniometer. After each measurement, the electrode was subsequently withdrawn from the cell and a new surface was generated, employing the same mechanical polishing routine mentioned above. The measurements were done both in a positive-going potential scan and in a negative-going potential scan. All of the experiments were carried out at ambient temperature (18$-$20 °C).

## Results and Discussion

**Cyclic Voltammetry Experiments.** Figure 1A shows the potentiodynamic *I*/*E* profiles as a function of the anodic potential

**TABLE 1: Electrical Charges Associated with Current Peak Contributions Obtained from Figure 1[a]**

| anodic contribution | $Q_A$ ($\mu$C cm$^{-2}$) | cathodic contribution | $Q_C$ ($\mu$C cm$^{-2}$) | $Q_A/Q_C$ |
|---|---|---|---|---|
| A1′ | 620 | C1′ | 670 | 0.93 |
| A1″ | 97 | C1″ | 100 | 0.97 |
| A2 | 151 | C2 | 154 | 0.98 |
| | | HER | | |

[a] $Q$ values were obtained from the respective deconvoluted $I/E$ voltammetric profiles.

limit ($E_{\lambda,a}$) of a bulk mechanically polished copper electrode, obtained in an unstirred borate buffered solution, pH 9.2, containing 1 mM EX$^-$. In the potential range from $-1.1$ to $-0.9$ V, a capacitive response is appreciated. By increasing the $E_{\lambda,a}$ values, complex positive (A1) and negative (C1) faradaic current contributions appear in the PGPS and NGPS, respectively. The shape of the current peak C1 and its current intensity depend on the $E_{\lambda,a}$ value fixed. Figure 1B and C show the different current contributions involved in the respective whole anodic (A1) and whole cathodic (C1) current peaks. These current contributions were obtained by deconvolution of the corresponding $I/E$ profile obtained when the $E_{\lambda,a}$ value was extended to $-0.6$ V. The deconvolution treatment was performed through a nonlinear curve-fitting program. Gaussian shapes for the peaks were considered. The result of deconvolution treatment for the PGPS (Figure 1B) show two anodic current peaks located at $-0.79$ V (A1′) and $-0.71$ V (A1″) and a current contribution that starts close to $-0.74$ V (A2). In the case of the NGPS (Figure 1C), three current peaks located at $-0.87$ V (C2), $-0.97$ V (C1″), and $-1.0$ V (C1′) are observed as well as an exponential cathodic current contribution assigned to HER.

The complementary current contributions assigned as A1′/C1′ and A1″/C1″ would correspond to the same electrochemical reaction but involve different copper sites that differ in their adsorption energy value for the [EX] radical, according to eq 4.

$$\mathrm{Cu} + \mathrm{EX}^- \underset{\mathrm{C1}}{\overset{\mathrm{A1}}{\rightleftarrows}} \mathrm{Cu[EX]_{ads}} + \mathrm{e}^- \qquad (4)$$

The different adsorption copper sites could correspond to crystallographic planes or surface defects that differ in nature and whose relevance of adsorption depends on the previous treatment of the surface electrode (see below).

The current contributions assigned as A2 and HER correspond to the formation of a Cu(I)−ethyl xanthate compound, represented as [CuEX], and the hydrogen evolution reaction according to eqs 5 and 6, respectively:

$$n\mathrm{Cu} + \mathrm{EX}^- \underset{\mathrm{C2}}{\overset{\mathrm{A2}}{\rightleftarrows}} \mathrm{Cu_{(n-1)}[CuEX]_{ads}} + \mathrm{e}^- \qquad (5)$$

$$2\mathrm{H_2O} + 2\mathrm{e}^- \rightarrow \mathrm{H_2} + 2\mathrm{OH}^- \qquad (6)$$

Reaction 5, which involves the formation of [CuEX], would occur in those copper sites not previously covered by ethyl xanthate radicals ([EX]).

The charge values obtained for each current contribution from Figure 1A and B as well as the $Q_A/Q_C$ ratio are shown in Table 1. The $Q_A/Q_C$ ratio was close to unity, indicating that the processes represented by reactions 4 and 5 are chemically reversible.

When the $E_{\lambda,a}$ values considered were more negative than $-0.6$ V, the corresponding fitting procedure of the respective $I/E$ profiles showed that the current contribution due to reaction 5 is lesser and disappears when the $E_{\lambda,a}$ value is more negative than $-0.75$ V (profiles not shown).

**TABLE 2: Anodic and Cathodic Electrical Charges and $Q_A/Q_C$ Ratios for A1 and C1 Processes Obtained from Figure 1A[a]**

| $E_{\lambda,a}$ (V) | $Q_A$ ($\mu$C cm$^{-2}$) | $Q_C$ ($\mu$C cm$^{-2}$) | $Q_A/Q_C$ |
|---|---|---|---|
| −0.60 | 743.4 | 732.5 | 1.02 |
| −0.65 | 572.2 | 597.7 | 0.96 |
| −0.70 | 491.4 | 506.6 | 0.97 |
| −0.75 | 331.6 | 324.3 | 1.02 |
| −0.80 | 142.1 | 149.4 | 0.95 |
| −0.85 | 43.7 | 47.4 | 0.92 |

[a] $Q_C$ values were obtained from the respective deconvoluted $I/E$ voltammetric profiles.

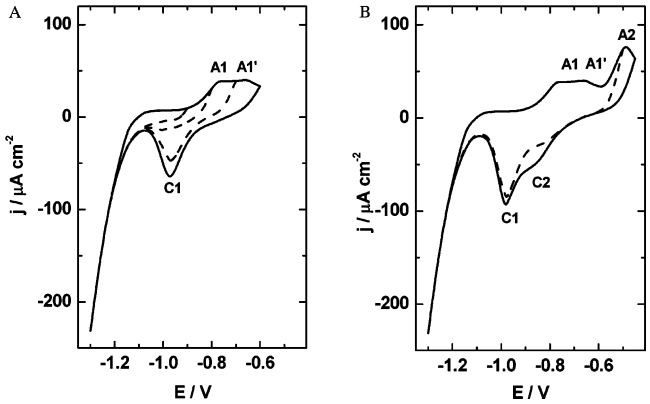


**Figure 2.** $I/E$ potentiodynamic profiles of a bulk copper electrode (chemically polished) in 50 mM borate buffer, pH 9.2, electrolyte solution containing 1 mM EX$^-$. Scan rate 0.02 V seg$^{-1}$. Potential range: (A) $-1.30$ to $-0.60$ V and (B) $-1.30$ to $-0.45$ V.

Besides, the inset of Figure 1A shows the behavior of a bulk copper electrode in the same electrolyte but in the absence of EX$^-$. It is important to note that the exponential current contribution due to HER is developed in a potential range where the anodic processes 4 and 5 are occurring. Therefore, it is reasonable to assume that all of these reactions take place simultaneously in this potential range.

Table 2 shows the $Q_A$ and $Q_C$ charge values obtained from the data of Figure 1 as a function of the $E_{\lambda,a}$ value attained in the PGPS. The $Q_C$ charge values were obtained by subtracting the HER charge values. Therefore, the $Q_C$ values reported involve the processes C1′ and C1″ (Figure 1C). Besides, Table 2 shows that the $Q_A/Q_C$ ratio is always close to 1.0 in accordance with the chemically reversible character of the anodic and cathodic electrochemical processes involved in the Cu/EX$^-$ system.

The effect of the surface treatment of a copper electrode on the potentiodynamic response under the experimental conditions described above is shown in Figure 2. In this figure, it is appreciated that the copper electrode (with a previous chemically polished treatment) shows two anodic signals, A1′ and A1″, in the PGPS. The respective maximal current peak of each one is located at $-0.77$ and $-0.66$ V, respectively. These potential values are coincident with the location of the current peaks obtained by deconvolution of the PGPS $I/E$ profile of Figure 1A. Furthermore, the current contribution A2 is developed as a current peak when the $E_{\lambda,a}$ value is extended beyond $-0.6$ V. Similarly, in the NGPS, it is appreciated that the complexity of the corresponding potentiodynamic $I/E$ profile depends on the anodic potential limit attained.

**Potentiostatic Experiments.** To prove that, depending on the potential considered, the HER is present during the elec-

**TABLE 3: Effect of the Stirring and the Adsorption Potential on the Negative Stationary Current and Cathodic Charge Values during the Polarization of the Interface Cu Electrode/50 mM Borate Buffer, pH 9.2, Containing 1 mM $EX^-$**

| | stationary current ($\mu$A) | | cathodic charge ($\mu$C) | |
|---|---|---|---|---|
| $E_{ads}$[a] (V) | unstirred | stirred | unstirred | stirred |
| −0.575 | 0.00 | 0.10 | 625.3 | 686.5 |
| −0.600 | 0.00 | 0.05 | 576.8 | 580.2 |
| −0.650 | −1.10 | −1.00 | 164.5 | 96.5 |
| −0.700 | −1.80 | −3.40 | 135.5 | 86.5 |
| −0.750 | −1.90 | −15.2 | 60.5 | 29.0 |
| −0.800 | −2.00 | −30.0 | 55.0 | 14.0 |
| −0.850 | −1.80 | −35.7 | 28.0 | 5.00 |
| −0.900 | −2.80 | −33.1 | 0 | 0 |

[a] Adsorption time of 4 min.

troadsorption of the EX radical, we applied a potentiostatic step at a value ($E_{ads}$) lying in the potential range from −0.900 to −0.575 V for 4 min. This potentiostatic step allowed the electroadsorption of the EX radical onto the copper electrode surface. The electrical charge associated with this process was evaluated from the respective *I*/*E* profile obtained when a NGPS was applied from the $E_{ads}$ value selected up to an $E_{\lambda,c}$ value of −1.30 V. It is important to remark that when $E_{ads}$ values were more negative than −0.65 V, the current measured at the end of the potential step was always negative and was enhanced by stirring the solution, as shown in Table 3. Because the experiments were carried out in an inert atmosphere and in the absence of species that would be reduced, the negative current observed is due to the HER, which occurs simultaneously with the electroadsorption of the EX radical. In stirred solutions and when the applied $E_{ads}$ value is more negative than −0.65 V, the HER prevails over other reactions.

The data of Table 3 reveal that the stirring conditions of the solution decrease the coverage of the copper electrode by the radical species of EX (reaction 4). As a consequence, an enhancement of the HER is observed due to an increase of the number of copper sites for the Volmer step in the HER, according to reaction 7:

$$Cu + H_2O + e^- \rightarrow Cu[H]_{ads} + OH^- \qquad (7)$$

Furthermore, in Table 3, it is appreciated that the HER is more evident when the $E_{ads}$ values are more negative than −0.65 V. On the contrary, at more positive potential values, this reaction does not occur and only the electrosorption of the EX radical and Cu(I)−EX compound formation take place (forward reactions 4 and 5, respectively). The latter is enhanced by stirring the solution. Besides, at potential values more negative than −0.90 V, only the HER is present.

**Electrochemical Quartz Crystal Microbalance (EQCM) Experiments.** To get additional information about the electrodesorption process of $EX^-$ species, the mass variation that occurs during the NGPS applied to a copper electrode, previously covered by the electrosorbed EX radical or Cu(I)−EX compounds, was determined by means of EQCM experiments. The EQCM technique has been recognized as an important tool for the study of mass variation that can take place on the electrode−solution interface during an electrochemical or adsorption/desorption process.[18]

The respective *I*/*E* and *m*/*E* profiles were obtained by using an electrodeposited copper film on a gold−quartz resonator acting as a working electrode. Initially, to reduce any oxygen-containing copper species present in the electrode surface, this electrode system was polarized at −1.30 V for 5 min. Then, a

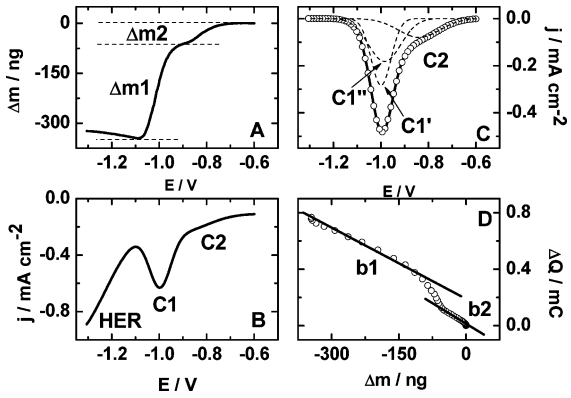


**Figure 3.** (A) *m*/*E* and (B) *I*/*E* potentiodynamics profiles. Interface: Au/Cu/50 mM borate buffer, pH 9.2, in the presence of 1 mM $X^-$. $E_{ads}$ = −0.575 V. $\tau_{ads}$ = 4 min, $\upsilon_c$ = 0.02 V $seg^{-1}$. (C) Deconvoluted *I*/*E* profile of part B without HER contribution. (D) Δ*Q* vs Δ*m* plot (Δ*Q* obtained from part C and Δ*m* obtained from part A).

potential step ($E_{ads}$) was applied for 4 min to provoke reactions 4 and 5. Afterward, a NGPS was carried out from this $E_{ads}$ potential value to −1.3 V. According to the $E_{ads}$ values established, the respective potentiodynamic *I*/*E* profiles obtained were deconvoluted in C1, C2, and HER processes (vide infra). As an example, Figure 3 shows the results obtained when an $E_{ads}$ value of −0.60 V was applied to the electrode system. The *m*/*E* profile (Figure 3A) exhibits two regions, assigned as Δ*m*2 and Δ*m*1, where a mass decrease takes place. In turn, the mass decreases are directly related to the respective electrochemical processes C2 and C1 of Figure 3B, both involving the departure of EX species from the electrode surface. In the potential range from −1.10 to −1.30 V of the NGPS, only the HER is present and the mass after attaining a minimum value gently increases. Figure 3C shows a deconvolution of the potentiodynamic *I*/*E* profile of Figure 3B but only considers the processes that involve a mass variation (departure of EX species). Besides, the C1 process contains the contributions C1′ and C1″ mentioned in the paragraph corresponding to CV experiments.

To confirm the EX species desorption during the NGPS, represented by the reverse of reactions 4 and 5, a Δ*Q*/Δ*m* plot is shown in Figure 3D. The data were obtained from Figure 3A and C. As it can be seen, two linear relationships with slopes $b_2$ and $b_1$ are established. Furthermore, a discontinuity in the plot is appreciated where an increase of the Δ*Q*/Δ*m* slope value is observed. The slope $b_2$ ($-2.3 \times 10^{-3}$ mC $ng^{-1}$) corresponds to the potential range from −0.60 to −0.85 V of the NGPS where the beginning of the C2 process (reverse reaction 5) principally occurs. Moreover, the slope $b_1$ ($-1.7 \times 10^{-3}$ mC $ng^{-1}$) corresponds to the potential range from −0.95 to −1.1 V of the NGPS where the C1 process (reverse of reaction 4) principally occurs. The discontinuity zone between the slopes $b_2$ and $b_1$ observed in the plot could be associated to copper loss from the electrode, during the occurrence of the C2 process. When the $E_{ads}$ values applied to the electrode were more negative than −0.60 V and did not involve the formation of a Cu(I)−EX compound (results not shown), the corresponding Δ*Q*/Δ*m* plots obtained showed a unique slope ($b_1$) with a value of $-(1.2 \pm 0.2) \times 10^{-3}$ mC $ng^{-1}$.

Taking into account the reverse reactions 4 and 5, which consider only the departure of EX species from the electrode, the theoretical value for the slope (*b*) should be $-8.0 \times 10^{-4}$ mC $ng^{-1}$. This value is less than that observed experimentally. This disagreement can be explained assuming that, depending on the $E_{ads}$ value applied, the electrode surface will be covered by EX radical species or a mixture of EX radical species and a

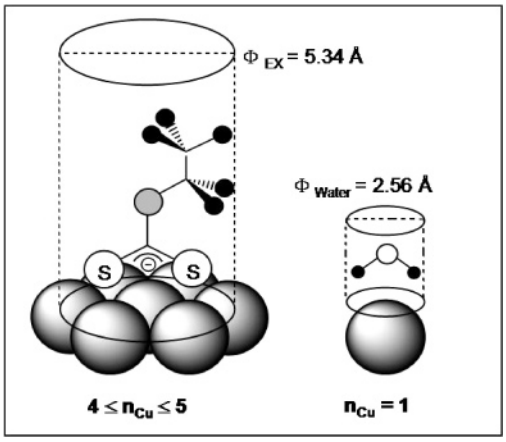


**Figure 4.** Graphic representation of the adsorption of the ethyl xanthate anion and water molecule on a copper surface.

Cu(I)−EX compound. Nevertheless, the coverage by EX radical species is always lower than a monolayer. It is important to note that this assumption is contrary to previous works where a monolayer of the EX radical was considered to be attained before the Cu(I)−EX compound was formed.[4,7] Therefore, during the imposed $E_{ads}$, there are copper sites prone to electrosorption of EX species (EX radical) and uncovered copper sites prone to electrooxidation to Cu(I)−EX species. Under the present experimental conditions ($E_{ads} = -0.60$ V), EX radical species and the Cu(I)−EX compound are formed and both cover the electrode surface. Therefore, when a NGPS is applied, they are reduced independently. The slope value $b_2$ ($-2.3 \times 10^{-3}$ mC ng$^{-1}$), corresponding to the reduction of the Cu(I)−EX compound, allows a molar mass of 41.95 g mol$^{-1}$ to be calculated. This value is smaller than 121.12 g mol$^{-1}$ corresponding to the molar mass of EX$^-$. The above suggests that, together with the departure of EX$^-$ anions from the electrode surface, the adsorption of water molecules would occur on those free copper sites left by the electrochemical process. Therefore, reaction 5 could be rewritten as follows:

$$Cu_{(n-1)}[CuEX]_{ads} + yH_2O + e^- \leftrightarrow nCu[H_2O]_{y(ads)} + EX^- \quad (8)$$

A value of $y = 4.4$ for the water molecules adsorbed, after the departure of one EX$^-$ anion from the electrode, is calculated by using eq 9:

$$y = \left[\frac{\left(\frac{F \times 10^{-6}}{b_2}\right) + MM_{EX^-}}{MM_{H_2O}}\right] \quad (9)$$

where $F$ is the Faraday constant, $b_2$ is $-2.3 \times 10^{-3}$ mC ng$^{-1}$, $MM_{EX^-}$ is the molar mass of the ethyl xanthate anion (121.12 g mol$^{-1}$), and $MM_{H_2O}$ is the molar mass of water (18 g mol$^{-1}$). The calculated $y$ value is close to those estimated from projection of both the molecular geometries of the EX$^-$ anion and the water molecule on the compact surface of copper, as illustrated in Figure 4.

According to Figure 4, four or five copper atoms can be covered by an EX species. Meanwhile, one copper atom is covered by a unique water molecule. In the calculations of the chemical species diameter (Φ), we employed the CS Chem Office software. The lowest energy state of both chemical species was considered in it. Besides, for the water molecule, we have represented only the angular adsorption because linear representation gave a similar result. An $n_{Cu}$ value of 4.4 was calculated considering an atomic radius of 1.278 Å for the copper atom. This value was the same as that obtained from the EQCM experiments.

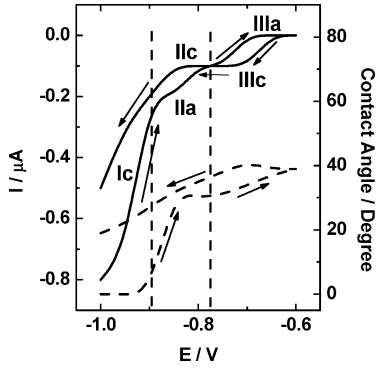


**Figure 5.** Polarization curves (continuous lines) and contact angle variation (dashed lines) for the PGPS and NGPS of a copper electrode in 50 mM borate buffer solution, pH 9.2, containing 1 mM EX$^-$.

On the other hand, the $b_1$ slope value of Figure 3B obeys the fact that, during the reduction of the electrosorbed EX radical, an important amount of the EX$^-$ anion that is generated remains specifically adsorbed on the electrode surface. Due to this, a minor mass decrease is detected in the process. The quantity of the EX$^-$ anion specifically adsorbed ($\theta - m$) is slightly dependent on the $E_{ads}$ established.

Therefore, the reverse of reaction 4 can be rewritten like eq 10:

$$Cu[\theta EX^-]_{ads} + \theta e^- \leftrightarrow Cu[(\theta - m)EX^-]_{ads} + (m)EX^-(aq) \quad (10)$$

where $\theta > m \geq 0.2\theta$ and $\theta < 1$.

**Electrochemical and Contact Angle Experiments.** To prove the change that the copper electrode surface suffers during its polarization in the presence of EX, contact angle measurements were performed. These measurements showed the modification of the hydrophilic/hydrophobic character of the electrode (or vice versa) that occurs when reactions 8 and 10 take place.

Figure 5 shows a stationary polarization curve done in PGPS and NGPS together with the simultaneous variation of the contact angle of an argon bubble disposed on the copper electrode surface. The contact angle measurement was made every 25 mV and after a stationary current value was attained for each chosen potential. Three regions appear clearly defined in the polarization curve obtained in the PGPS, and they are denoted as Ic, IIa, and IIIa, respectively. It is important to note that, in the respective *I*/*E* profile registered, both PGPS and NGPS, all of the current values are negative, indicating that the HER prevails over any other electrochemical process that is occurring in the potential range recorded. The regions IIa and IIIa correspond to forward reactions 4 and 5, which appear overlapped in the process Ic corresponding to the HER (reaction 6). In the potential range where the HER occurs exclusively ($-1.0$ to $-0.93$ V) the contact angle value is constant and close to zero, denoting a hydrophilic character of the electrode surface. Toward more positive potential values than $-0.9$ V, a wave is developed related to the electrosorption of EX radicals. Consequently, an important increase of the contact angle value occurs, revealing that the electrode surface turns to a hydrophobic character. In the region IIIa, which is extended from $-0.8$ to $-0.6$ V, a second wave appears related to the formation of the Cu(I)−EX compound. The contact angle continues increasing, and the hydrophobic character of the electrode

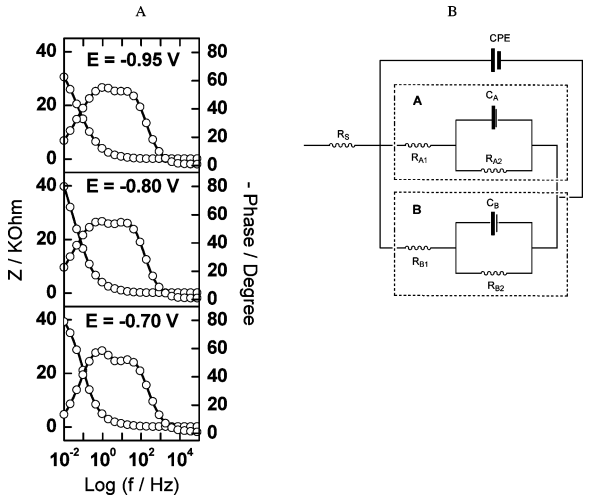


**Figure 6.** (A) Bode diagrams for the copper electrode in 50 mM borate buffer, pH 9.2: (—) experimental data; (○) fitted data. (B) Equivalent circuit.

surface does too. This behavior reveals that the hydrocarbonated chain of both the EX radical and the Cu(I)−EX compound formed face preferentially toward the solution, in accordance with what was previously described by Bozkurt et al.[5] During the NGPS, two waves assigned as IIIc and IIc appear in the potential range from −0.6 to −0.9 V, that correspond to the reduction of the Cu(I)−EX compound (reaction 8) and the desorption of the EX radical (reaction 10), respectively. Nevertheless, wave IIc is not completely resolved due to the overlapping of HER. In the potential range from −0.6 to −0.7 V, during the NGPS, the contact angle remains constant. Then, the contact angle decreases monotonically together with the hydrophobic character of the electrode surface, due to the occurrence of the reactions mentioned above. The most remarkable fact is that a zero value of the contact angle is not attained and the corresponding cathodic current is lesser than the value observed once the initial potential of −1.0 V is imposed again. These facts reveal that a specific adsorption of the $EX^-$ anion would occur on copper sites, which provoke both a residual hydrophobicity of the surface and a decrease of HER, simultaneously.

**Electrochemical Impedance Spectroscopy Experiments.** To gain insight about HER, which is always present during the electroadsorption of the EX radical on copper electrodes, electrochemical impedance measurements were performed in the presence and absence of the $EX^-$ anion in the electrolyte. This study was carried out in the potential range from −0.70 to −0.95 V. In the absence of the $EX^-$ anion, the following reaction scheme for the HER on a conductor substrate was considered.[19−21]

$$M + e^- + H_2O \rightarrow M{-}H + OH^- \quad (11)$$

$$2M{-}H \rightarrow 2M + H_2 \quad (12)$$

$$M{-}H + e^- + H_2O \rightarrow M + H_2 + OH^- \quad (13)$$

where M represents a substrate site and M−H represents hydrogen adatoms adsorbed on M. In the present work, M corresponds to copper sites that could differ in adsorption energy for hydrogen adatoms.

Figure 6A shows the Bode plots obtained for a copper electrode in a borate medium in the absence of the $EX^-$ anion (continuous line). These plots show that, in the frequency range studied, the phase angle measurements exhibit two capacitive contributions. These contributions are better resolved when the potential applied to the electrode increases from −0.95 to −0.70 V.

The experimental data were analyzed using a nonlinear fit according to the following expression:

$$Z_T = R_S + Z_{TF} \quad (14)$$

$$Z_{TF} = \left(\frac{1}{Z_A} + \frac{1}{Z_B} + \mathrm{CPE}_{dl}\right)^{-1} \quad (15)$$

$$Z_A = \left(\frac{1}{R_{A2}} + j\omega C_A\right)^{-1} + R_{A1} \quad (16)$$

$$Z_B = \left(\frac{1}{R_{B2}} + j\omega C_B\right)^{-1} + R_{B1} \quad (17)$$

$$[\mathrm{CPE}_{dl}] = (C_{dl}(j\omega)^{\alpha})^{-1} \quad (18)$$

where $\omega = 2\pi f$ and $R_S$ denotes the ohmic resistance of the system. $Z_T$ is the transfer function of the system, which is represented by the equivalent electric circuit shown in Figure 6B. This equivalent circuit takes into consideration the electrochemical reactions of eqs 11−13. A very good concordance between the experimental data with simulated data (open circles in Figure 6A) is appreciated. The transfer function contains the impedances corresponding to the subcircuits A and B, which are similar because they would represent the occurrence of the HER on copper surface sites that would differ in crystallographic planes or correspond to surface defects of a different nature. Therefore, different adsorption energies are expected for the hydrogen adatom adsorption. The elements $R_{A1}$ and $R_{B1}$ represent the reaction resistance for pathway 11. $C_A$ and $C_B$ are the capacitances due to the existence of hydrogen adatoms formed in this pathway. The elements $R_{A2}$ and $R_{B2}$ represent the reaction resistance that would correspond to a chemical reaction (pathway 12) or an electronic transfer reaction (pathway 13).

Table 4 shows values of different contributions to the total impedance. In both subcircuits A and B, independent of the potential applied, the corresponding $R_{A1}$ and $R_{B1}$ values (pathway 11) are lower than the resistances $R_{A2}$ and $R_{B2}$ (pathway 12 or 13); this indicates that the first charge transfer is not the limiting step for the HER. Nevertheless, the highest values found for $R_{A1}$, with respect to $R_{B1}$, reveal that the electroformation of hydrogen adatoms on copper sites A is less favorable than on copper sites B. This fact is evident in the Bode diagram because two capacitive contributions appear clearly established. The capacitive contribution located at the lowest frequency would correspond to the HER that occurs on the copper sites A.

In the presence of the $EX^-$ anion, the Bode plots obtained are shown in Figure 7A. In this figure, two contributions which appear clearly defined in the potential range from −0.95 to −0.70 V are appreciated. At more positive potential values, the phase angle for the signal that appears at lower frequencies ($10^{-1}$ Hz) decreases. However, the magnitude of the phase angle for the signal that appears at high frequencies remains constant in the potential range considered. It is possible to assume that the last signal corresponds to the HER because the angle value is similar to the one observed in the absence of the $EX^-$ anion.

**TABLE 4: Equivalent Circuit Parameters for the Copper Electrode (0.3 cm$^2$) in 50 mM Borate Buffer, pH 9.2, at Different Applied Potentials**

| | | CPE | | copper sites A | | | copper sites B | | |
|---|---|---|---|---|---|---|---|---|---|
| $E$ (V) | $10^2R_S$ (Ω) | $C_{dl}$ ($\mu$F cm$^{-2}$) | α | $R_{A1}$ (KΩ) | $C_A$ ($\mu$F cm$^{-2}$) | $R_{A2}$ (KΩ) | $R_{B1}$ (Ω) | $C_B$ ($\mu$F cm$^{-2}$) | $R_{B2}$ (KΩ) |
| −0.95 | 1.3 | 16.6 | 0.6 | 6.71 | 31.8 | 38.9 | 8.13 | 17.7 | 360 |
| −0.80 | 1.4 | 15.5 | 0.6 | 10.0 | 37.0 | 59.8 | 9.49 | 19.9 | 468 |
| −0.70 | 1.4 | 19.3 | 0.7 | 5.34 | 43.9 | 47.3 | 16.5 | 8.75 | 335 |

**TABLE 5: Equivalent Circuit Parameters for the Copper Electrode (0.3 cm$^2$) in 50 mM Borate Buffer, pH 9.2, Containing 1 mM EX$^-$ at Different Applied Potentials**

| | | | | system A | | | system B | | |
|---|---|---|---|---|---|---|---|---|---|
| | | CPE | | | $CPE_{EX}$ | | | | |
| $E$ (V) | $10^2R_S$ (Ω) | $C_{dl}$ ($\mu$F cm$^{-2}$) | α | $R_{EX}$ (KΩ) | $C_{EX}$ ($\mu$F cm$^{-2}$) | $\alpha_{EX}$ | $R_{H1}$ (Ω) | $C_H$ ($\mu$F cm$^{-2}$) | $R_{H2}$ (KΩ) |
| −0.95 | 1.3 | 79.3 | 0.8 | 2.17 | 171.9 | 0.8 | 20.3 | 4.16 | 44.4 |
| −0.80 | 1.4 | 61.1 | 0.8 | 4.91 | 222.8 | 0.8 | 21.4 | 3.10 | 82.2 |
| −0.70 | 1.3 | 71.5 | 0.7 | 9.55 | 213.3 | 0.8 | 234 | 6.93 | 87.4 |

The experimental data were once again analyzed using a nonlinear fit. In this case, the following expressions were considered:

$$Z_T = R_S + Z_{TF} \tag{19}$$

$$Z_{TF} = \left(\frac{1}{Z_A} + \frac{1}{Z_B} + \mathrm{CPE}_{dl}\right)^{-1} \tag{20}$$

$$Z_A = \frac{1}{\mathrm{CPE}_{EX}} + R_{EX} \tag{21}$$

$$Z_B = \left(\frac{1}{R_{H2}} + j\omega C_H\right)^{-1} + R_{H1} \tag{22}$$

$$[\mathrm{CPE}_{dl}] = (C_{dl}(j\omega)^{\alpha})^{-1} \quad \text{and} \quad [\mathrm{CPE}_{EX}] = (C_{EX}(j\omega)^{\alpha_{EX}})^{-1} \tag{23}$$

$Z_T$ is the transfer function of the system, which is represented by the equivalent electric circuit shown in Figure 7B. The present equivalent circuit takes into consideration reaction 4 (system A) and reactions 11−13 (system B).

A very good concordance between the experimental data (continuous line) with simulated data (open circles in Figure 7A) is appreciated. $R_{EX}$ and $C_{EX}$ in system A correspond to a resistance of the electron transfer of reaction 4 and a capacitance due to the adsorption of EX radicals on the copper surface electrode, respectively. For system B, the elements named $R_{H1}$, $C_H$, and $R_{H2}$ have already been described above. The values of the different elements in the equivalent circuit of Figure 7B are shown in Table 5.

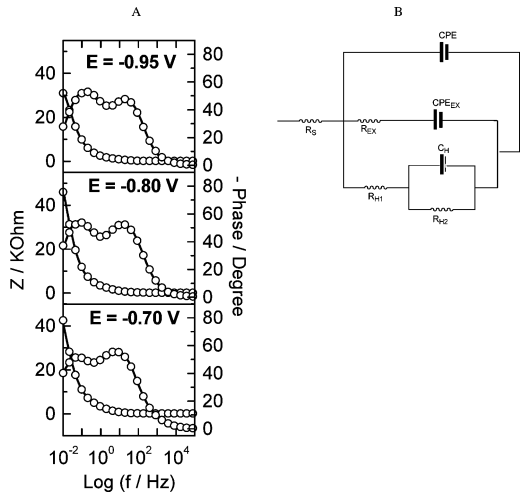


**Figure 7.** (A) Bode diagrams for the copper electrode in 50 mM borate buffer, pH 9.2, containing 1 mM EX$^-$: (—) experimental data; (○) fitted data. (B) Equivalent circuit.

Table 5 shows that $R_S$ and $C_{dl}$ values remain nearly constant at the potentials assayed. Nevertheless, the $C_{dl}$ values are greater than the corresponding values obtained in the absence of the EX$^-$ anion, because the adsorption of the EX radical is present now. The $R_{H1}$ values increase with the potential, because of the available sites for the HER decrease due to the partial coverage of the copper surface by EX electroadsorption, which takes place simultaneously. Moreover, the HER is not favored with the increase of the potential. On the other hand, the $C_H$ values are slightly diminished by the EX adsorption. It is observed that the $R_{H2}$ parameter increases with the potential and its value is higher than the parameter $R_{H1}$, which was similarly observed in the absence of EX. Therefore, the mechanism of the HER is not affected by the presence of EX in the electrolyte.

With respect to system A, it is observed that the $R_{EX}$ and $C_{EX}$ parameters are both increased when the potential value is more positive. This behavior is due to an increase of $\theta_{EX}$ with the potential. In consequence, a decrease of the available free surface sites ($1 - \theta_{EX}$) takes place for the electroadsorption process.

## Conclusions

From the potentiodynamic and EIS measurements performed in the potential range from −0.80 and −0.60 V, two parallel reactions were characterized. These reactions were the ethyl xanthate electroadsorption and the hydrogen evolution reaction, respectively.

The EIS measurements allow establishing that the mechanism of the HER on copper electrodes is not affected by the presence of an ethyl xanthate species.

The EQCM study shows that in the electrodesorption process the departure of each ethyl xanthate species from the copper electrode is accompanied with the simultaneous entry of four to five water molecules. This fact is in accordance with the number of the copper atoms involved in the adsorption of one ethyl xanthate species.

**Acknowledgment.** The financial support of Fondecyt through contract 2010007 and DI-PUCV are gratefully acknowledged by the authors. P.G. acknowledges the doctoral fellowships granted by Conicyt-Chile.

## References and Notes

(1) Crozier, R. D. *Flotation. Theory, Reagents and Ore Testing*; Pergamon Press: New York, 1992; Chapters 3 and 4.

(2) Chander, S.; Fuerstenau, D. W. *Electroanal. Chem. Interface Electrochem.* **1974**, *56*, 217.

(3) Woods, R. *J. Phys. Chem.* **1971**, *75*, 354.

(4) Woods, R.; Young, C. A.; Yoon, R. H. *Int. J. Miner. Process.* **1990**, *30*, 17.

(5) Bozkurt, V.; Xu, Z.; Brienne, S. H. R.; Butler, I. S.; Finch, J. A. *J. Electroanal. Chem.* **1999**, *475*, 124.

(6) Hepel, M.; Scendo, M. *J. Electroanal. Chem.* **2002**, *538*−*539*, 121.

(7) Mielczarski, J.; Werfel, F.; Suoninen, E. *Appl. Surf. Sci.* **1983**, *17*, 160.

(8) Woods, R.; Basilio, C. I.; Kim, D. S.; Yoon, R.-H. *Int. J. Miner. Process.* **1994**, *42*, 215.

(9) Woods, R. *Aust. J. Chem.* **1972**, *25*, 2329.

(10) Woods, R.; Basilio, C. I.; Kim, D. S.; Yoon, R. H. *J. Electroanal. Chem.* **1992**, *328*, 179.

(11) Buckley, A. N.; Parks, T. J.; Vassallo, A. M.; Woods, R. *Int. J. Miner. Process.* **1997**, *51*, 303.

(12) Leppinen, J. O.; Basilio, C. I.; Yoon, R. H. *Int. J. Miner. Process.* **1989**, *26*, 259.

(13) Chander, S.; Khan, A. *Int. J. Miner. Process.* **2000**, *58*, 45.

(14) Guo, H.; Yen, W.-T. *Miner. Eng.* **2003**, *16*, 247.

(15) Shchukarev, A. V.; Kravets, I. M.; Buckley, A. N.; Woods, R. *Int. J. Miner. Process.* **1994**, *41*, 99.

(16) Buckley, A. N.; Woods, R. *Int. J. Miner. Process.* **1990**, *28*, 301.

(17) Kowal, A.; Pomianowski, A. *Electroanal. Chem. Interface Electrochem.* **1973**, *46*, 411.

(18) Hepel, M. *Electrode*−*Solution Interface Studied with Electrochemical Quartz Crystal Nanobalance, in Interfacial Electrochemistry. Theory, Experiments and Applications*; Wieckowsky, A., Ed.; Marcel Dekker: New York, 1999; pp 599−630.

(19) Barber, J. H.; Conway, B. E. *J. Electroanal. Chem.* **1999**, *461*, 80.

(20) Bockris, J. O. M.; Khan, S. U. M. *Surface Electrochemistry, A molecular Approach*; Plenum Press: New York, 1993; pp 310−316.

(21) Córdova, R.; Gómez, H.; Schrebler, R.; Cury, P.; Orellana, M.; Grez, P.; Leinen, D.; Ramos-Barrado, J. R.; Del Río, R. *Langmuir* **2002**, *18*, 8647.